HermesB: A Continuous Neural Recording System for Freely Behaving Primates

Gopal Santhanam, Michael D. Linderman, *Student Member, IEEE*, Vikash Gilja, Afsheen Afshar, *Student Member, IEEE*, Stephen I. Ryu, Teresa H. Meng, *Fellow, IEEE*, and Krishna V. Shenoy*, *Senior Member, IEEE*

***Abstract*—Chronically implanted electrode arrays have enabled a broad range of advances in basic electrophysiology and neural prosthetics. Those successes motivate new experiments, particularly, the development of prototype implantable prosthetic processors for continuous use in freely behaving subjects, both monkeys and humans. However, traditional experimental techniques require the subject to be restrained, limiting both the types and duration of experiments. In this paper, we present a dual-channel, battery-powered neural recording system with an integrated three-axis accelerometer for use with chronically implanted electrode arrays in freely behaving primates. The recording system called HermesB, is self-contained, autonomous, programmable, and capable of recording broadband neural (sampled at 30 kS/s) and acceleration data to a removable compact flash card for up to 48 h. We have collected long-duration data sets with HermesB from an adult macaque monkey which provide insight into time scales and free behaviors inaccessible under traditional experiments. Variations in action potential shape and root-mean square (RMS) noise are observed across a range of time scales. The peak-to-peak voltage of action potentials varied by up to 30% over a 24-h period including step changes in waveform amplitude (up to 25%) coincident with high acceleration movements of the head. These initial results suggest that spike-sorting algorithms can no longer assume stable neural signals and will need to transition to adaptive signal processing methodologies to maximize performance. During physically active periods (defined by head-mounted accelerometer), significantly reduced 5–25-Hz local field potential (LFP) power and increased firing rate variability were observed. Using a threshold fit to LFP power, 93% of 403 5-min recording blocks were correctly classified as active or inactive, potentially providing an efficient tool for identifying different behavioral contexts in prosthetic applications. These results demonstrate the utility of the HermesB system and motivate using this type of system to advance neural prosthetics and electrophysiological experiments.**

***Index Terms*—Electrode recording stability, freely behaving electrophysiology, neural prostheses, neural recordings.**

Manuscript received October 24, 2006; revised February 4, 2007. G. Santhanam and M. D. Linderman contributed equally to this work. The work of M. D. Linderman and T. H. Meng was supported by the Focus Center Research Program Center for Circuit and System Solutions (www.c2s2.org) under Contract 2003-CT-888. The work of V. Gilja, M. D. Linderman, and G. Santhanam was supported by the National Defense Science and Engineering Graduate (NDSEG) fellowship. The work of G. Santhanam was also supported by the National Science Foundation (NSF). The work of A. Afshar was supported by the Medical Scientist Training Program and the Bio-X fellowships. The work of S. I. Ryu and K. V. Shenoy was supported by the Christopher Reeve Paralysis Foundation. The work of K. V. Shenoy was also supported by the following awards from NSF Center for Neuromorphic Systems Engineering at Caltech, the ONR Adaptive Neural Systems, the Whitaker Foundation, the Center for Integrated Systems at Stanford, the Sloan Foundation, and the Burroughs Wellcome Fund Career Award in the Biomedical Sciences. *Asterisk indicated the corresponding author.*

G. Santhanam, M. D. Linderman, and T. H. Meng are with the Department of Electrical Engineering, Stanford University, Stanford, CA 94305 USA (e-mail: gopals@stanford.edu; mlinderm@stanford.edu; thm@stanford.edu).

V. Gilja is with the Department of Computer Science, Stanford University, Stanford, CA 94305 USA (e-mail: gilja@stanford.edu).

A. Afshar is with the Department of Electrical Engineering and the Medical Scientist Training Program, Stanford University, Stanford, CA 94305 USA (e-mail: afsheen@stanford.edu).

S. I. Ryu is with the Department of Electrical Engineering and the Department of Neurosurgery, Stanford University, Stanford, CA 94305 USA (e-mail: seoulman@stanford.edu).

*K. V. Shenoy is with the Department of Electrical Engineering and the Neurosciences Program, 319 CISX, 330 Serra Mall, Stanford University, Stanford, CA 94305 USA (e-mail: shenoy@stanford.edu).

Digital Object Identifier 10.1109/TBME.2007.895753

I. Introduction

THE development of chronically implantable electrode arrays for *in vivo* neural recording in primates (both monkeys and humans) has enabled a range of advances, in neural prostheses [1]–[6] and basic electrophysiology experiments [7]–[9]. However, most current state-of-the-art experimental systems require the animal to be restrained, restricting both the types and duration of experiments. As a result there is limited data available with which to characterize both the nature and content of neural recordings over the broader range of time scales and free behaviors relevant to future prosthetic and electrophysiology experiments. To make the transition to new experimental paradigms possible, continuous, long-duration, broadband [sampled as 30 kS/s (kilosamples per second)] neural recordings from freely behaving subjects are needed. These data sets will enable validation of spike discrimination and decoding algorithm performance in freely behaving subjects, multiday plasticity and learning experiments, determination of neural correlates of free behaviors, and direct measurement of the stability of neural recordings. In this paper, we present results from the hours of electrophysiological recordings in monkey with an extensible system, version B (the whole system was nicknamed HermesB), addressing the latter two questions to demonstrate the utility of long-duration recording from freely behaving subjects.

Recording stability is a critical issue for neural prosthetic systems. Here, we define recording stability, or more specifically, recording instability, as change in the gross presence or absence of neural signals off an electrode, time-varying fluctuations of the observed action potential shape, and time-varying fluctuations in the background noise process on an electrode. Neural recordings during any given session are considered to be quasi-stable; there is usually very little change in the numbers of

0018-9294/$25.00 © 2007 IEEE

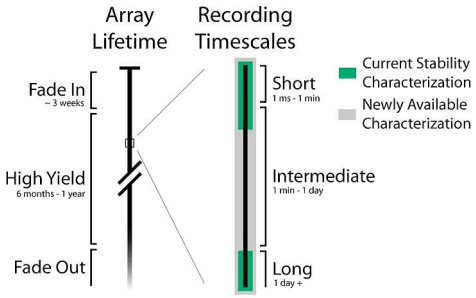

Fig. 1. Summary of array lifetime and available data for recording from individual, identifiable neurons using a chronically implanted electrode array.

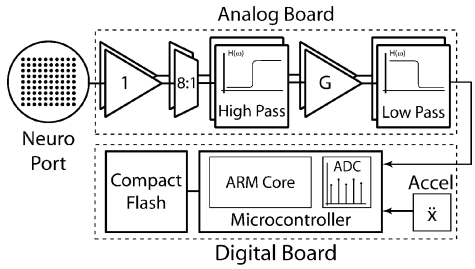

Fig. 2. HermesB block diagram. The neuroport is a custom 96 channel zero insertion force connector which mates to the electrode array connector. The analog signal conditioning and digitization and storage are implemented on separate circuit boards to reduce noise and provide modularity.

neurons recorded and their action potential shapes during a several hour recording session. However, recording instability has been observed between sessions, likely resulting from the subjects freely behaving in the housing room between sessions [10]. Long-durations data sets will enable us to reconcile the current assumptions of quasi-stable neural signals during a highly controlled experimental session with the variation in the neural signals observed between sessions.

Fig. 1 summarizes the significant time scales in the life of a chronically implanted electrode array. In this paper, we are only concerned with neural recording stability in the high-yield recording period during which most experiments are conducted [11]. Within this window, neural interface systems are potentially affected by recording instability at all three time scales (short, intermediate, and long). However, current experiments, with their discrete daily recording periods, are only able to characterize variations on time scales less than a few hours or across days. Thus, past studies have only characterized neural recording stability on short (e.g., seconds or minutes [10], [12]) and long time scales (e.g., days [10], [13], [14]). Over very short time scales, observed variations in action potential waveform shape are a function of the short-term spiking frequency of a neuron [12]; at high frequencies, the waveform is typically broader (in time) and decreased in amplitude due to depletion of ion gradients in and around a highly active neuron. At longer time scales, the variation in spike waveform is not as systematic, potentially arising from a number of mechanisms such as neural plasticity, physical movement of the electrode relative to nearby neurons, chemical degradation of the electrode tip, or immunological reactions to the implant [11], [15]. Studying neural stability at intermediate time scales will enable characterization (along with existing short and long time scale data) of the full range of time scales relevant to a neural interface system and may also provide insight into long time scale phenomena.

Experimental protocols in which the subject is retrained limit the types of behaviors that can be observed. Long-duration data sets recorded during free behavior provide neural data associated with a broader range of behaviors than traditionally possible. To maximize system performance, prostheses must be sensitive to behavioral and neural changes across the day and must react robustly in the face of variable background conditions. For example, such systems should reliably detect different behavioral contexts such as whether the user is awake or asleep, or intends to be active or not. If a neural prosthetic attempts to decode the users intentions during sleep, it may waste battery power or cause undesired behaviors. Alternatively, if such a system does not reliably detect waking periods, the user may lose the ability to interact with the world. The ability to record neural activity across a variety of different behaviors and contexts will be allowed for characterization of the true neural environment in which chronic implantable systems will operate.

Long-duration data sets are of considerable interest for certain multiday electrophysiology experiments. Chronically implanted electrode arrays can support multiday learning or plasticity experiments. However, because the time between traditional daily recording periods is unobserved, there is no reliable method to track single neurons over multiple days. Recording systems for freely behaving subjects can allow researchers to record while the animal is in its home cage, providing continuous monitoring of neurons identified during an active experiment. Without such monitoring, it is not possible to certify that the same neuron is being observed day-to-day and thereby reliably state that the adaption is not the result of recording instability in the system.

Recording systems have been developed for freely behaving animals [16]–[18]. However, these systems often have one or more of the following limitations: 1) they cannot sample at full broadband (30 kS/s), potentially missing relevant signal features; 2) their battery life or storage capacity is limited to a few hours or less for broadband recording; 3) they cannot switch recording parameters, such as input channel, autonomously, limiting the range of possible experiments; and 4) they are not designed or tested for portable use with primates.

In this paper, we describe the first generation of a portable recording system, dubbed HermesB. HermesB addresses the limitations of previous systems by providing a full broadband, long-duration, autonomous recording platform for use with chronically implanted electrode arrays in primates. An extensible system, HermesB can easily evolve to include new components such as experimental analog front ends (e.g., [19]), making HermesB a useful prototyping platform as well. Importantly, the system interfaces (although not exclusively so) with the popular 96 channel electrode array manufactured by Cyberkinetics Neurotechnology, Inc. (CKI, Foxborough, MA). This implant has been adopted by many electrophysiology research laboratories and is now Federal Drug Administration (FDA) approved for clinical trials with humans [6]. Understanding the characteristics of this array and the stability of

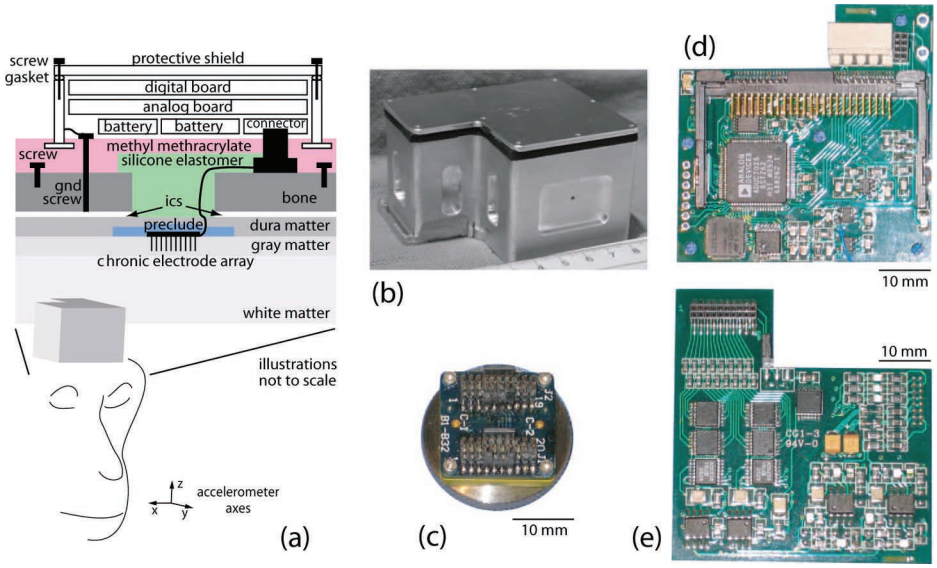

Fig. 3. HermesB components. (a) Illustration of enclosure mounted on monkey's head along with side profile showing the stack up of the various components. The space labeled ICS denotes the intracranial space between the dura and skull. This space is larger in humans compared to monkeys and may be a source of greater recording variability when electrode-based systems transition to the clinical domain. (b) Aluminum enclosure with centimeter ruler. (c) Custom low-profile neuroport connector. (d) Digital board. (e) Analog board.

signals recorded from it can provide great benefit for translating the technology to the clinical setting.

To demonstrate the utility of HermesB, we present preliminary results derived from multiday broadband recordings from a freely behaving macaque monkey which provide insight into previously unobserved time scales and behavioral contexts. A macaque was chosen as it is generally accepted as the ideal animal model for researching neural prostheses for humans [1]–[5], [20]–[22]. In particular, we present data quantifying the stability of neural recordings over time scales from 5 min to 54 h. We address three aspects of recording stability identified in [15]: the change in mean waveform shape over time, changes in the background noise process, and changes in the waveform shape due to electrode movement. We illustrate the ability to identify contextual periods in our long-duration neural recordings and specific attention is paid towards identifying and understanding systematic differences in firing rate and local field potential (LFP) during active and inactive periods.

TABLE I
HERMESB PARAMETERS

Interface Capabilities	
Simultaneous active channels	2
Programmably accessible channels	16
Connector accessible channels	96
3-axis accelerometer range	±6G
Storage	currently 6 GB
Physical Parameters	
Enclosure size	60x70x45 mm
Enclosure mass	127 g
Electronics mass incl. batteries	77 g
Neuroport mass	16 g
Grand total mass	220 g
Signal Conditioning Parameters	
High pass filter (-3dB)	< .5 Hz
Low pass filter (-3dB)	7.4 kHz
Neural sampling rate	30 kSamples/s
Accel. sampling rate	1 kSamples/s
ADC Precision	12 bits
Battery Parameters	
Battery Capacity	1600 mAh
Typical Battery Life at 67% recoding duty cycle	19 hrs
Measured Circuit Parameters	
Input referred noise	3.5 μV RMS
Input referred precision	1 μV per LSB
Amplifier Gain	∼610×

II. METHODOLOGY

A. System Description

The HermesB system is composed of three distinct modules, a custom 96-pin neural microconnector, an analog signal conditioning module, and a digital signal acquisition unit. A block diagram of the HermesB recording system is shown in Fig. 2. The system and its placement on the animal are shown in Fig. 3. The schematics for the analog and digital modules are shown in Fig. 13. System specifications are summarized in Table I.

1) System Overview: The HermesB is architected to be a flexible, modular, extensible experimental platform. Although capable of interfacing with any electrode array, the current HermesB system is designed to work with the 96-channel chronic electrode array manufactured by CKI (wired to a CerePort™ connector pedestal). The HermesB system provides two independent neural recording channels and a three-axis accelerometer. The two neural recording channels are selected electronically from a subset of 16 channels, with the particular 16 of the 96 selected mechanically through interchangeable printed circuit boards (PCBs). The neural and acceleration data is digitized and written to a nonvolatile type I compact flash card (CF).

2) Neural Connector: The space available on the animal's head limits the size of the neural interface connector. Thus, although the electrode array provides 96 channels, only a subset of channels can be physically accessed at one time. Commercially available connectors are too large for a compact self-contained implementation, requiring a custom design. A low-pro-

file zero-insertion-force (ZIF) connector was developed, shown in Fig. 3(c). The new connector is comprised of a mechanical component which allows access to all 96 electrodes and a set of three PCBs interface that provide access to 32 channel subsets (PCBs are interchanged manually). Of those 32, a subset of 16 is selected with a second PCB for input to the analog module.

3) Analog Module: The analog signal conditioning path is shown in the upper dashed box of Figs. 2 and 3(e) [schematics are shown in Fig. 13(a)]. The necessary amplification and filtering is determined by the characteristics of neural signals recorded from chronic silicon electrode arrays. Neural signals have strong spectral power content up to 8 kHz, thus a minimum sampling rate of 15 kS/s is required. In the HermesB system, as in many commercial systems, we chose to oversample (30 kS/s) to relax the specifications for the antialias filter.[1] All 16 accessible electrode channels undergo immediate impedance conversion using a unity gain source follower complimentary metal–oxide–semiconductor (CMOS) op–amp (TLC2254, Texas Instruments, Dallax TX). The electrodes have a high impedance (100–300 kΩ), which must be reduced to control noise. The desired channels are digitally selected using 8 : 1 analog multiplexers (ADG658, Analog Devices, Norwood, MA). After the multiplexers, the selected signals are passively high-pass filtered with a cutoff of 0.5 Hz to remove electrode dc bias [which would otherwise exceed the analog-to-digital converter (ADC) dynamic range]. The main amplification stage uses differential instrumentation amplifiers (Texas Instruments INA121) with gain of 98.8. Three path-matched references are provided—two reference signals and analog ground—selectable via a jumper. The two references are platinum–iridium reference wires that accompany the electrode array and provide an electrical reference local to the implantation site. Afterward, the signals were actively low-pass filtered with a cutoff 7.5 kHz and amplified with a gain of $\sim$6.2 (using Texas Instruments OPA2344). The 7.5-kHz cutoff ensures all of the important spectral content is preserved, while providing excellent suppression at the Nyquist frequency. Resistor and capacitor values and filter topologies are shown in the schematics. The total gain is determined by the ADC dynamic range (2.5 V) and the maximum amplitude of the local field potential (estimated at 3000 μV).

4) Digital Module: The digital module is shown in the lower dashed box of Figs. 2 and 3(d) [schematics are shown in Fig. 13(b)]. Neural signals are digitized at 30 kS/s by a 12-bit successive approximation ADC integrated in the ARM microcontroller, which is clocked at 22.5 MHz (Analog Devices ADUC2106). The dynamic range for the ADC is 2.5 V, which with the total gain of 610 provides an input referred resolution of 1 μV/lsb for the neural signals. The $\pm$6 g three-axis accelerometer (ST Microsystems STM9321) is mounted on the digital board. Each accelerometer channel is also digitized by the microcontroller at 1 kS/s and has a nominal resolution of 0.003 g/lsb. The HermesB system is controlled by custom firmware written in C.

[1]Rack-mounted commercial systems (which are not power limited) typically use sampling rates in 30–40-kS/s range. In addition to relaxing the required order of the antialias filter, the higher sampling rate reduces the need to interpolate and align spike snippets during postprocessing. To ensure maximum performance, however, we continue to interpolate and align, even with the higher sampling rate.

```
% Setup the sampling frequncy to be 30 kHz
% on the neural channels and sample the
% accelerometer once every 30 neural samples.
%
% Initial 600 sec standby period followed
% by loop of 300 sec. of recoding from
% channels 4 & 6 and 150 sec. of standby
neuralfreq 30000                  % Line 0
accelperiod 30                    % Line 1
addsleep 600                      % Line 2
addsample 4 6 300                 % Line 3
addsleep 150                      % Line 4
addloop 3                         % Line 5
```

Fig. 4. Sample program for autonomous execution. The initial standby period is added to allow the experimenters sufficient time to close up the protective enclosure before recording commences.

5) Software Control: The firmware includes a simple command interpreter which allows the user to interact with the system in real time when tethered to a portable computer (via RS-232 serial port), as well as write simple sequencing programs for autonomous execution. A sample program is shown in Fig. 4. The system is highly configurable. Parameters such as neural sampling rate and accelerometer sampling rate can be set to balance sampling precision against data storage capacity. The experimenter can then specify a sequence of epochs, each either a data sampling period or quiescent standby period, to balance data set continuity against battery lifetime.

6) Power Supply: The positive and negative power supplies are provided by separate lithium ion batteries (*positive:* LG Chem ICP633450A1; $49.0 \times 33.6 \times 6.8$ mm^3; 24.3 g; 4.2 V; 1120 mAh; *negative:* Varta EasyPack; $43.5 \times 35.4 \times 5.8$ mm^3; 14 g; 4.2 V; 570 mAh). The 3.3-V digital supply voltage and 2.5-V analog supply voltage are provided by linear voltage regulators (LTC1844 series, Linear Technology, Milpitas, CA). The $-$2.5-V analog supply voltage is provided by a third linear regulator (Linear Technology LT1961). HermesB draws a constant 5.3 mA from the negative battery and 38.8, 11.4, and 71 mA from the positive battery during idle upon reset, standby, and active sampling periods, respectively.

7) Physical Construction: The entire system is housed in a lightweight, protective aluminum case, shown in Fig. 3(a) and (b), secured with methyl methacrylate, which was in turn secured to the skull. The enclosure was sealed with a watertight gasket and grounded to the monkey to provide electromagnetic (EM) shielding for the electronics. The electronics are tightly packed in the case with nonconductive foam to prevent vibration, shown in Fig. 3(a).[2] The entire system weighs 200 g, which is light enough that no behavioral differences were observed (ensuring collected data represents natural behavior).

8) Limitations and Future Work: The tight space, weight, and power constraints force a number of design limitations on the HermesB system. However, many of these limitations can

[2]Thus, we can safely state that our accelerometer records head motion and not any residual board vibrations.

be addressed in future designs by leveraging improving commercial-off-the-shelf (COTS) technology, or recently developed neural recording specific integrated circuits.

The number of neural channels is determined by the footprint of an analog signal path. In the present design, only two channels could fit within the available space (the size of which is set by the animal's head). Future versions of the HermesB system can replace the current discrete analog signal paths with soon to be available custom integrated circuits (such as [19]) enabling 16 or more channels to be recorded simultaneously within the same overall footprint. Although not needed for the current system (since only two channels can be recorded simultaneously), more channels than the current 16 can be made available by replacing the current connector PCB and headers with a more dense design.

The ability to digitally select among the 16 channels enables time multiplexing of the neural recording paths. However, the switching speed is limited by the slow dynamics of the large capacitor in the 0.5-Hz high-pass filter. More complex circuits are under development to increase switching speed for the current analog signal path. Switching speed is not a problem for the integrated analog front end approach which uses independent per-channel amplifiers and filters.

The system is very sensitive to the write latency of the compact flash card. "Fast" cards intended for use in high-end digital cameras are required to supply the necessary write bandwidth. However, the capacity and performance of CF cards is constantly improving allowing the capabilities of HermesB to scale as well without redesign or remanufacturing. In future designs, the CF recording will be supplanted by wireless transmission to eliminate storage limitations and enable real-time interaction.

By utilizing modular construction (separate analog and digital PCBs) and standard interfaces like CF, the HermesB system can be easily upgraded. The future work would only require replacement of the analog module or the substitution of a CF form factor wireless transceiver for the current flash card. Additional ADC channels are available to support new analog data sources, such as chronically implanted electromyogram (EMG) electrodes.

B. Recordings and Analyses

Primary data for this report was collected from an adult female macaque monkey (monkey D) freely moving in a home cage. All experiments and procedures were approved by the Stanford University Institutional Animal Care and Use Committee (IACUC, Stanford, CA). We performed a sterile surgery to implant a head restraint system. At this time, we also implanted a silicon 96-electrode array. The electrode array (Cyberkinetics, Foxborough, MA) was implanted in a region spanning the arm representation of the dorsal aspect of premotor cortex (PMd) and primary motor cortex (M1), as estimated visually from local anatomical landmarks. Surgical methods are very similar to that described in [9].

HermesB was used to record starting in August 2005. A number of recording profiles were used. One profile consisted of recording at a 67% duty cycle (5 min of recording followed by 2.5 min of standby). Total experiment duration was approximately 54 h, broken up into three 18-h sessions. The duty cycling is a compromise between memory capacity and battery life constraints. When recording continuously, the current memory capacity can be quickly exhausted. At very low duty cycling, the battery is discharged by the static power consumption before the CF card is full, despite putting the microcontroller in standby between recording blocks. Between each session, the monkey was transferred from the home cage to the training chair to replace the battery and download the $\sim$4 GB of recorded data. During these "pit stops," recording was continued with a second smaller CF card and new battery to maintain data set continuity. Other profiles include round-robin recording of 4–8 channels over a 24-h schedule. Two neural channels were recorded per data set in full broadband (0.5 Hz to 7.5 kHz at 30 kS/s with 12-bit resolution) and a three-axis accelerometer fixed to the monkey's head was sampled (1 kS/s with 12-bit resolution) and stored to compact flash.

Accelerometer data was used from each 5-min data block to label the blocks as either "active," "inactive," or "mixed." Blocks in which the maximum accelerometer magnitude (MAM) was greater than 1.25 g were labeled active, blocks in which the MAM was less than 1.15 g were labeled inactive, and blocks that were within these bounds were labeled mixed. These thresholds were selected to roughly balance the number of active and inactive blocks with the ratio of day (lights on) versus night (lights off) blocks (as we expect low activity when the lights are off), while retaining a 0.1-g margin between classifications.

The recorded neural signals from each 5-min block were postprocessed with the Sahani spike-sorting algorithm, which is an unsupervised clustering algorithm [23], [24]. Spike times were identified using a threshold determined from data across the block (3σ with respect to the RMS noise estimate from filtered data). A spike waveform, or snippet, comprised of a 32-sample window around the threshold event, and was extracted and aligned to its center of mass (COM). Snippets were projected into a 4-D robust, noise-whitened principal components space (NWrPCA) and clustered using a maximum *a posteriori* (MAP) clustering technique. Well-isolated units were identified and cross referenced across blocks by hand. For LFP analyses, broadband data was filtered by applying Chebyshev type I low-pass and bandpass filters with a passband ripple of 1 dB. Power spectral density estimates were calculated using the Welch periodgram method.

C. Recording Stability Analyses

To quantify the stability and consistency of waveforms recorded from our electrode array, we analyzed data from our long-duration recordings in several ways. First, snippets from the entire session were extracted using a 3σ threshold and projected into a single 2-D principal components subspace. By graphing a 2-D histogram of the snippets in this subspace, snippets with similar waveform shapes are grouped into distinct clusters. Movement of these clusters across the session indicates drift in the waveforms. The magnitude of the shifts were then assessed by examining the actual waveform shapes over these periods of interest. Second, to observe more continuous

shifts in waveform shape, we chose a feature of the average waveform shape, the peak-to-peak voltage (V_{pp}), and plotted this quantity over the course of the recording session. The V_{pp} was determined on a block-by-block basis by using the Sahani algorithm per block, providing local estimates of the average waveform shapes.

Last, to search for potentially abrupt changes in waveform shape, the neural recordings were analyzed in conjunction with the accelerometer data. An abrupt change in electrode array position in the cortex would presumably manifest itself as an abrupt change in waveform amplitude, as the neuron–electrode distance would change. If such changes do occur, we additionally presume they are correlated with high acceleration events such as vigorous head movement. Therefore, we examined the neural recordings straddling high acceleration events (>3 g threshold) and examined the V_{pp} metric around these events. To help search for events of interest, we computed the local change of the V_{pp} metric ($V_{pp}^{\text{after}}/V_{pp}^{\text{before}}$), constructed from 200 snippets before and 200 snippets after the acceleration event. This allowed us to narrow in on high acceleration events that coincided with large shifts in action potential waveform shape.

Single neural units were used for these analyses to observe the recording stability from our chronic implant. One important concern is that if a unit is automatically identified by the spike sorter, large changes in the unit's waveform shape could cause the unit to no longer be classified correctly, thereby obscuring the analyses. Thus, the NWrPCA projections of the selected units were examined separately by the experimenters to ensure that snippets were not ignored or improperly included. This was accomplished by ensuring all units included in the aforementioned stability analyses were well-isolated, high-firing-rate single neurons, and sufficiently distinct from other signals on their respective electrodes such that reasonably large variations would not result in a high rate of misclassification.

III. Results

A. System Verification

Fig. 5 shows example data recorded from our animal subject freely moving in her home cage. The top traces [Fig. 5(a)] show the three-axis acceleration of the monkey's head over a 10-s period. This data segment was recorded in the early evening during a period in which the monkey was quite active. Fig. 5(b) shows 100 ms of broadband neural data recorded from a single channel on the electrode array. The LFP is easily visible as is a number of spikes "riding" on top of the LFP. Fig. 5(c) shows the same data segment filtered with a 250-Hz high-pass infinite impulse response (IIR) filter, which is the same filter used for spike sorting.

Data sets, like that shown in Fig. 5, were used as part of a three step verification process to ensure the accuracy of HermesB recordings. The steps were as follows: 1) measure HermesB circuit parameters, 2) compare recordings of the CKI Neural Simulator made with HermesB and our standard laboratory recording system (CKI Cerebus System), and 3) compare HermesB recordings of neural activity in a rhesus monkey to recordings made by the fixed laboratory system.

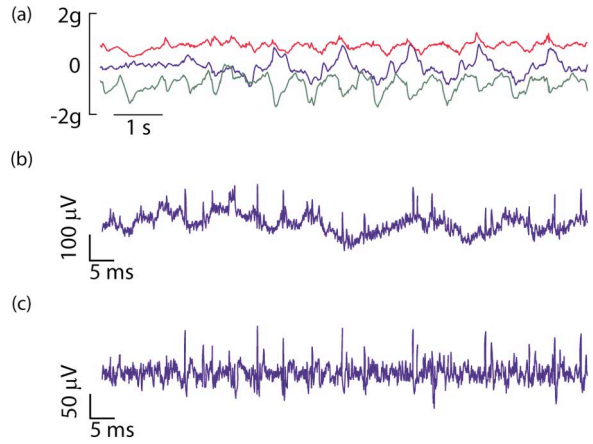

Fig. 5. Sample neural and accelerometer data recorded from a freely behaving monkey. (a) Accelerometer channels: x (blue), y (green), and z (red). The direct current (dc) levels on the channels are due to the particular orientation of the accelerometer with respect to Earth's gravity vector. (b) Unfiltered broadband neural data taken from the middle of the recording period. (c) Filtered broadband neural data.

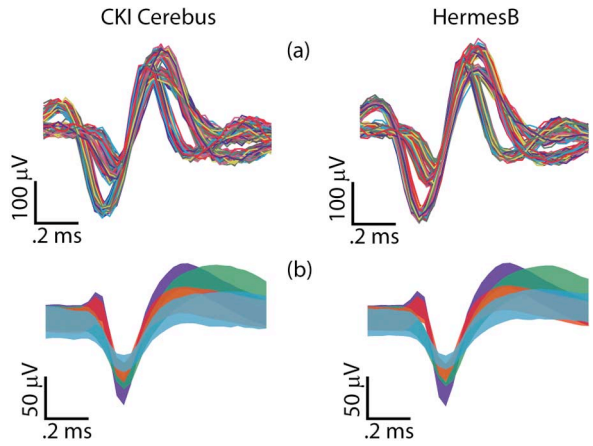

Fig. 6. Comparison of snippets recorded with CKI Cerebus system (left) and HermesB (right). (a) Snippets recorded from CKI Neural Simulator. (b) Snippets from four neurons recorded from a single electrode channel in a monkey comfortably in a chair with head restrained. Snippets have been sorted and the 10th–90th percentile in amplitude indicated by the colored region for each waveform.

The measured circuit parameters are summarized in Table I. The input referred noise, measured with grounded inputs, is comparable to or better than current state-of-the-art commercial (CKI Cerebus System) and research systems [19]. The CKI Neural Simulator is a neural recording playback device that provides 128 channels of simulated neural signals at typical amplitudes for array recordings (e.g., maximum of ~500 μV peak-to-peak for spikes) and similar output impedance to a standard electrode array. Fig. 6(a) shows a side-by-side comparison of Neural Simulator recordings made with the CKI Cerebus system (left) and with HermesB (right). The three spike waveforms are clearly visible, with comparable levels of noise (measured as the spread of the curves) between the two systems. Fig. 6(b) shows a similar comparison for a channel from the electrode array, recorded from a monkey sitting quietly in a primate chair. The figure shows the 10th–90th percentile in amplitude of action potential waveforms recorded from a single

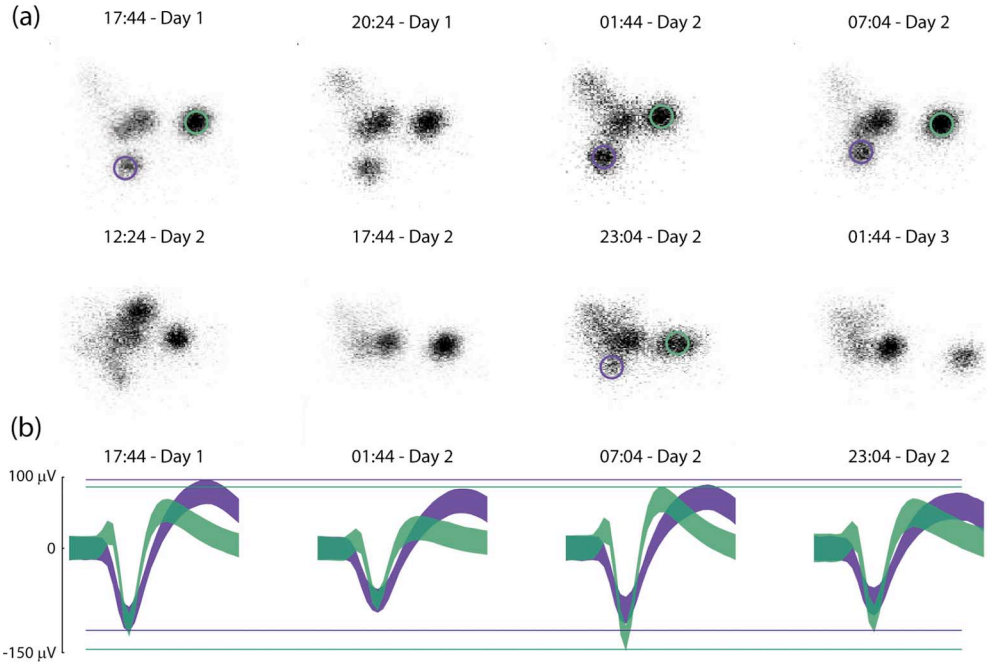

Fig. 7. Neural recordings over a period of 48 h (data set `D20051008`). (a) Histogram of spike waveform projections into a fixed 2-D NWrPCA space. PCA space determined using 20 000 snippets uniformly selected across the time period. Each plot is the projection of 5 min of data recorded from a signal channel at the time shown. The green and blue circles denote identifiable single neurons that are analyzed in the bottom panel. (b) Spike waveforms of two neurons for selected 5-min blocks. To better isolate the selected units, spike sorting was performed strictly within a block and irrespective of the data in other blocks. Colored region indicates 10th–90th percentile in amplitude. Horizontal lines indicate maximum and minimum voltage for each unit. Waveforms shown are recorded from a single channel using the same signal conditioning path. Note that between 17:44 (day 1) and 07:04 (day 2) V_{pp}, the peak-to-peak voltage of the green waveform increases, while V_{pp} of the blue waveform decreases, showing that waveform changes cannot be attributed to fluctuations in signal conditioning pathway (connectorization, amplifiers, ADC, battery power, etc.).

channel on the electrode array. A 5-min recording was sorted using the Sahani algorithm which classified the spikes as belonging to one of four units (indicated by different coloring). There were four separable units. The spike snippets were projected into a lower dimensional subspace to verify that they originated from separable clusters (data not shown). The waveforms are very similar between the two systems, indicating that HermesB is comparable to current state-of-the-art commercial laboratory equipment. Furthermore, the ability of HermesB to distinguish between several units on a single electrode builds confidence that this apparatus can serve to address the scientific goals posed earlier in this paper.

B. Recording Stability

Fig. 7 shows neural recordings made over the course of 48 h in October 2005. Fig. 7(a) shows a time series of NWrPCA cluster plots for 5-min data segments recorded at the times shown. Each cluster corresponds to a single neuron, and the movement (drift) of the relative distance between these clusters is readily seen by scanning across the snapshots. The drift of the clusters in NWrPCA space reflects changes in spike waveform shape. Fig. 7(b) shows action potential shapes (voltage versus time) from the same recording period. The colored region indicates the 10th–90th percentile in amplitude. The lines of constant voltage provide a reference against which one can see the large changes in waveform amplitude. These changes in action potential shape have been previously observed across once-daily recordings [10]. Here, preliminary results from these continuous neural recordings of a freely behaving primate indicate substantial variation in spike waveforms over intermediate time scales as well.

Fig. 8 shows a more continuous representation of the waveform changes over time. Fig. 8(c) shows the normalized peak-to-peak voltage for the neuron identified in Fig. 8(a), recorded from a single channel over 54-h periods. The normalized V_{pp} is simply the mean V_{pp} for each block, normalized by V_{pp} of the mean waveform for that neuron across the entire 54-h data set. Variability in waveform amplitude, up to 30% relative to the mean, is observed over a range of time scales. There is a clear variation on the order of a single block (5-min recording with 2.5 min of standby) as well as changes on the order of several blocks, and even several hours. Fig. 8(d) shows the RMS voltage of filtered neural recordings from the same channel. All spikes, identified with thresholding at 3σ of RMS noise, have been removed from the data set prior to the RMS calculation shown. Without the spikes, the RMS value should offer a better measure of the true background noise process [25]. Even after removing identifiable spikes, the RMS noise is correlated to neural activity (as measured by mean firing rate).[3] These variations ($\sim$5 μV) can partly result from distant spike activity (i.e., neural activity is sensed by the electrode, but the signal does not rise above the

[3]The RMS voltage rises on average during the day and falls during the night. The neural activity, shown for the same neurons in Fig. 11(d) and (g), follows a similar pattern (higher firing rate during the day when the animal is awake, less at night). Since nearby neural activity contributes to the RMS noise, the correlation is expected, as the firing rate of nearby neurons is likely correlated with the firing of the unit under consideration.

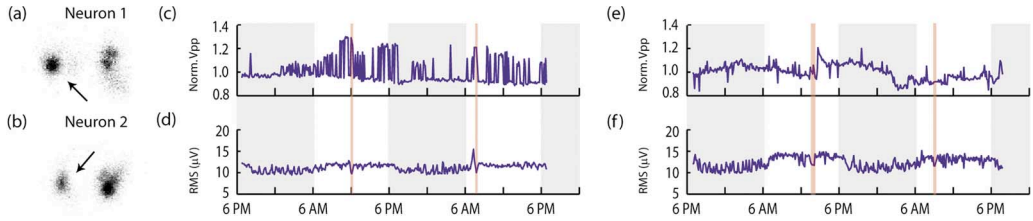

Fig. 8. Variation in V_{pp} and RMS. (a) and (b) Histogram of spike waveform projections into NWrPCA space from two different electrodes recorded for different 54-h data sets (`D20060225.ch1` and `D20060302.ch2`). Selected neurons are indicated by arrows. These neurons were well isolated. (c) Normalized V_{pp} of neuron #1 recorded over the 54-h session. (d) RMS noise of recorded channels over same period. (e) and (f) Same two plots second data set. The wide light gray regions indicate night and the thin pink regions indicate "pit stops," when the monkey was taken from the home cage and placed in a primate chair to service the recording equipment.

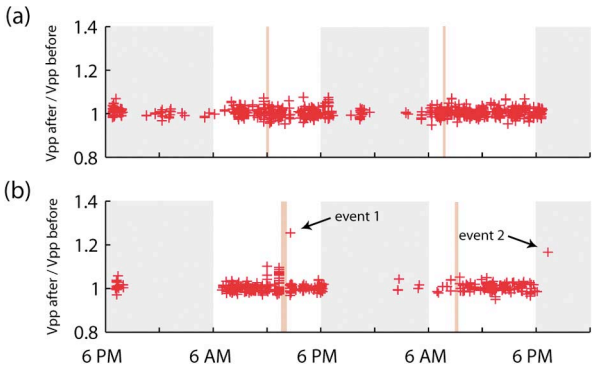

Fig. 9. Variation in waveform amplitude straddling high acceleration events. (a) Local change in mean waveform amplitude ($V_{pp}^{\text{after}}/V_{pp}^{\text{before}}$) for 200 snippets before and after 3^+ g acceleration events (data set `D20060225.ch1u1`). (b) Same as previous panel for data set `D20060302.ch2u1`. Arrows in (b) indicate events of interest. Similar gray and pink shading as in Fig. 8.

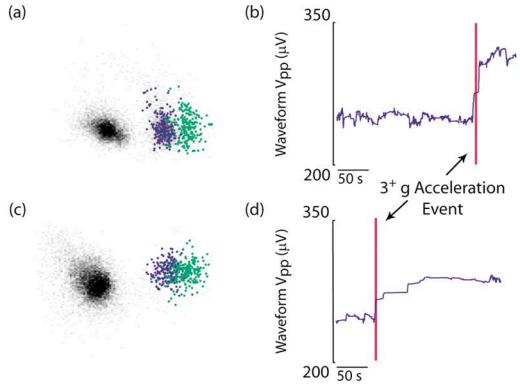

Fig. 10. Variation in waveform amplitude for events identified in Fig. 9(b). (a) NWrPCA projection of 200 before (blue) and 200 after (green) snippets straddling acceleration event overlaid on NWrPCA histogram for all snippets in 5-min block. Data set `D20060302.ch2`. (b) Peak-to-peak voltage of mean waveform amplitude averaged over 200 spikes centered around time point shown, for the neuron of interest in (a). The red vertical line marks the >3 g acceleration event. (c) and (d) Similar plots for event 2 in the same data set.

spike threshold because the spike amplitude is to small or the neuron is too far away). Furthermore, depending on which data block is analyzed to set the threshold, there can be differences greater than 15 μV for a 3σ threshold. Fig. 8(e) and (f) shows similar results for the neuron identified in Fig. 8(b) which was recorded from a different electrode during a different 54-h period. Similar characteristics have been observed for other channels (data not shown), indicating that the changes in waveform amplitude observed in Fig. 8(c) and (e) are not unique to those channels. The large change observed at 13:00 (day 1) in Fig. 8(e) is coincident with a vigorous head movement, and may have resulted from abrupt movement of the array (a possibility discussed in the following section).

In our analysis of abrupt waveform changes, examination of recordings straddling high acceleration events show, in nearly all cases, far smaller changes in waveform amplitude than those observed over the intermediate time scales of Fig. 8. For example, Fig. 9(a) and (b) shows the local changes in $V_{pp}(V_{pp}^{\text{after}}/\text{V}_{pp}^{\text{before}})$ for all 3^+ g acceleration events for the same two neurons in Fig. 8(c) and (e). Over a recording period of 50 h for each session, there were $\sim$1700 and $\sim$800 high acceleration events for Fig. 9(a) and (b), respectively.

For nearly all events shown in Fig. 9(a) and (b), there is less than a 5% change in mean waveform amplitude straddling the acceleration event. There are, however, two events in Fig. 9(b) that show much larger changes (labeled event 1 and 2). For the first of these events, the NWrPCA projections of the before (blue) and after (green) snippets for the events indicated by the arrows are shown in Fig. 10(a). The significant change in waveform amplitude (1.25 $\times$ increase) is clearly reflected in the NWrPCA projection. A second unit on this channel (the other cluster in the NWrPCA projection) shows a smaller change in amplitude (only a 1.1 $\times$ increase) across the same acceleration event suggesting that the observed variation does not result from changes in the signal conditioning pathway (not shown). For example, a common shift in signal gain would result in equivalent waveform amplitude change for both units, which was not the case here.

Fig. 10(b) shows a 200 spike moving average of V_{pp} for the block in which the event was recorded. The close alignment between the acceleration event (indicated by the red vertical line) and the step change in waveform amplitude strongly suggests that the relationship between the change in waveform amplitude and the high acceleration event is not coincidental. The profile is consistent with an abrupt change in array position. Well before and after the shift, the array was in a stable state, evidenced by the near-constant waveform amplitude, while at the time of the large acceleration event there is a step change in the V_{pp}. Fig. 10(c) and (d) shows similar results for the second event in Fig. 9(b).

The same analysis was repeated for a larger set of channels and neurons, compromising $\sim$84 h of recording. Many tens of events showed $>$10% change in average waveform amplitude coincident with a $>$3-g acceleration measurement.

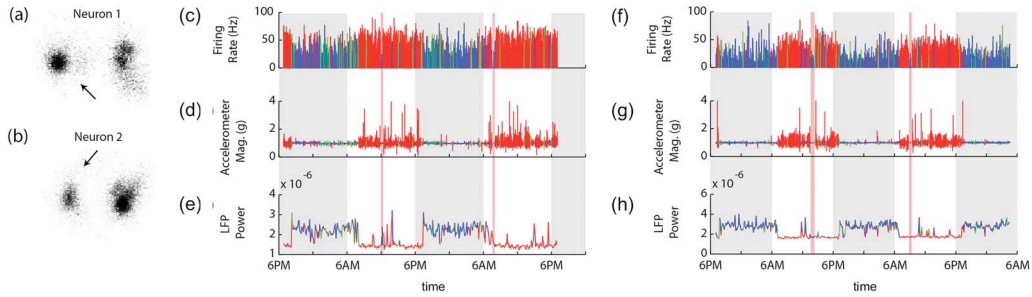

Fig. 11. Neural and accelerometer data recorded from a freely behaving monkey. (a) and (b) Histogram of spike waveform projections into NWrPCA space from two different electrodes recorded for different 54-h data sets (`D20060225.ch1` and `D20060302.ch2`). Selected neurons are indicated by arrows. These neurons were well isolated. (c) Firing rate of the neuron shown in (a) calculated over a 1-s interval using a Hamming window. Red and blue data points were recorded in time periods labeled as "active" and "inactive," respectively. Green data points were recorded during unlabeled periods. (d) Accelerometer magnitude over the recording period downsampled to 100 Hz. (e) LFP power per block, recorded from the same electrode, calculated by integrating the power over the 5–25-Hz frequency band. (f)–(h) Same plots for second data set. Similar gray and pink shading as in Fig. 8.

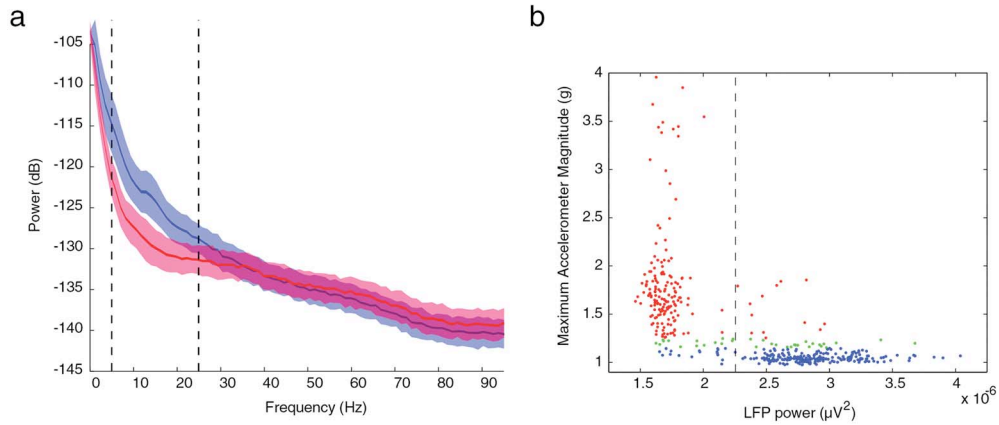

Fig. 12. LFP analyses for data set `D20060302.ch2`. (a) Power spectral density (PSD) recorded during "active" (red) and "inactive" (blue) periods. The thin lines are the mean PSDs and the standard error of the mean is represented by their thickness. The thickness of the wider translucent lines are the standard deviations. Each PSD is calculated over 5 min of data and their distributions were taken from data across the 54-h data set for neuron 1. (b) Spectral power recorded during "active" (red) and "inactive" (blue) periods for the 5–25-Hz frequency band. The dotted line represents the learned classification threshold between "active" and "inactive" blocks.

C. Neural Correlates of Behavioral Contexts

Fig. 11 shows data from two 54-h recordings. For the neuron 1 data set [presented in Fig. 11(a) and (c)–(e)] there were 438 data blocks. Active blocks, in which the monkey was putatively moving in its home cage, constituted 40% of the blocks while 52% of the blocks were inactive. From the accelerometer data [Fig. 11(d)], it is clear that the monkey is more physically active during the day, and as expected, firing rates tend to be higher during these periods. Note that LFP power was generally lower during these periods as shown in Fig. 11(e). During the "pit stops" (battery swap periods) the monkey's head was comfortably restrained in a fixed position (the time duration indicated by the pink bands); therefore, accelerometer magnitude remained flat at 1 g. Likewise, few movements were made, and consequently, firing rates were suppressed. These trends were consistent across two data sets collected from different electrodes and at different times. Neural activity recorded from a second channel show similar patterns [Fig. 11(b) and (f)–(h)].

As shown in Fig. 12(a), the mean LFP power differed between "active" and "inactive" periods in the 2–30-Hz and 50–100-Hz frequency bands. For the majority of this range, the standard deviations are large relative to the difference in the mean; this relationship makes power modulation in these bands an unreliable classifier for per-block behavior (i.e., "active" versus "inactive"). However, the 5–25-Hz band was well separated, so the power in this range can be used to develop a reliable classifier. This differentiation in LFP power was observed across multiple channels and multiple days, and is consistent with previous results showing that 10–100-Hz LFP activity diminished during movement [26], [27] and increased during sleep [28].

Fig. 12(b) plots 5–25-Hz LFP power versus MAM for each 5-min block. When we classified the activity level of blocks by thresholding LFP power at −56.5 dB, 93% (131/141) of "active" blocks and 92% (175/191) of "inactive" blocks were correctly classified. Results were similar for a second channel for a different session: 89% (150/169) of "active" blocks and 88% (81/92) of "inactive" blocks were correctly classified with a threshold of −57.1 dB. These results were obtained by picking the optimal linear classification boundary using the first 40 active and first 40 inactive blocks and testing on the remaining blocks. Head posting during "pit stops" can create confound since the accelerometer was held in a fixed position even if the monkey was otherwise active during these periods. Hence, these periods were removed prior to the aforementioned analysis.

A similar classification was not as successful when using the average firing rate over a 5-min block (data not shown). The mean and variance of the MAM increased as the firing rate increased, but the likelihood of a small MAM (i.e., an inactive period) remained relatively high even for high firing rates (data

not shown). Recall that the electrode was implanted in a region spanning PMd and M1, which is strongly believed to be involved in motor planning and execution of arm movements [29]–[34]. If arm movements are made while the head position remains fixed, firing rates could increase without large acceleration events. Also, motor plans can be generated and subsequently canceled. Thus, absolute firing rate may not be the best proxy for activity level.

Given that "active" and "inactive" periods tended to occur during day and night, respectively, the variations in firing rate and LFP might be explained, in part, by circadian rhythms (or direct modulation by light level). One might hypothesize that 5–25-Hz LFP power is increased and firing rates are depressed in association with day–night cycles. However, for blocks within a single activity condition (either "active" or "inactive"), the differences between day and night for both LFP and firing rate were at least an order of magnitude smaller than the difference between "active" and "inactive" blocks during either time period. This suggests that circadian rhythms do not heavily influence these effects.

IV. Discussion

In this paper, we report HermesB, a new, self-contained, long-duration, neural recording system for use with freely behaving primates. HermesB records dual channel broadband and three-axis head acceleration data to a high density compact flash card. Controlled by simple sequencing programs written by the experimenter, HermesB can autonomously change recording channel and pause recording during the experiment. With a single battery charge, HermesB can record for up to 48 h (at a low duty cycle). With short breaks to replace the batteries and compact flash card, HermesB can record nearly continuously for an indefinite period.

The high quality of the broadband recordings, despite being in the electrically noisy environment of the home cage room (e.g., florescent lights), enables results from HermesB to be integrated into experiments using the traditional laboratory rig. There are varieties of applications for such a platform. For example, the long-duration recordings, in concert with traditional experiments, enable important multiday learning and plasticity experiments, an application not explored in detail in this paper. Researchers can use HermesB to record during periods when the animal is outside the rig to provide continuous monitoring of significant neurons identified during active experiments.

To demonstrate the utility of HermesB, we analyzed the first set of multiday broadband neural and accelerometer data from area PMd in a freely behaving primate. In one set of analyses, we showed how HermesB can be useful in exploring the different neural contexts of a freely behaving subject. Practical neural prosthetic systems need to work well under varied conditions. We can begin to understand these conditions as contexts, defined here as a set of behavioral states and/or goals (such as active versus inactive or keyboard typing versus free-hand drawing). A switch in context may change the dynamics of observed neural signals and a neural prosthetic must be sensitive to these changes.

We examined a very simple pair of contexts—physically active and inactive. The monkey moved freely, so we could register these periods with an accelerometer. For an immobile patient, however, we would have to determine the *intent* to be physically active or inactive. As shown in Fig. 12, LFP is a promising proxy for activity level. Firing rate can also be used for this purpose. However, LFP power measurement consumes less battery power than firing rate measurement (a low-power LFP power measurement circuit is described in [35]), potentially enabling a power efficient implant "standby" mode when the user is inactive. When LFP power falls below a defined threshold, indicating that the user is, or intends to be, active, the prosthetic can switch out of this "standby" mode. Furthermore, using LFP thresholding could help prevent undesired movements from the prosthetic system during "inactive" periods.

In future studies, we plan to examine subtler context changes. Some contexts may require fewer neurons for acceptable performance; under these conditions, we can conserve power by disabling a subset of the neural channels. Under different contexts, users may require different sets of behavioral responses (such as discrete target selection versus continuous motion) or the underlying dynamics of the observed cortical area may change drastically; we would like to respond to these concerns by switching the decoding model according to context. By identifying contexts and adjusting hardware configuration accordingly, it may be possible to boost performance in terms of power consumption and decoding accuracy.

We were able to identify natural behavior across multiple days using accelerometer measurements and correlating these to neural recordings. Such an ability coupled with more advanced behavioral monitoring, such as chronically implanted EMG electrodes [36], [37] or motion tracking, can enable the exploration of questions that have been unapproachable until now. Mining large data sets of free behavior to find neural correlates may help us develop new controlled experiments; these data sets are also necessary for testing and developing neural prosthetics systems with the ability to operate autonomously over extended periods of time. Similar investigations are already underway by other researchers and HermesB can serve as another tool in these types of experiments [38], [39].

Our most novel investigation were our analyses of neural recording stability. It is in this particular class of experiments that HermesB is most differentiated from other portable recording systems currently in use. In particular, we addressed three aspects of recording stability identified in [15] and listed earlier: the change in mean waveform shape over time, changes in the background noise process, and changes in waveform shape due to electrode array movement. Initial analysis shows significant nonabrupt variation in waveform amplitude and RMS noise at intermediate time scales, along with step changes in waveform amplitude coincident with high acceleration movements of the head. Although some of these instabilities have been observed previously (or speculated), they have not been specifically, quantitatively measured. The results presented here provide preliminary characterization of neural recording stability, providing a meaningful starting point for both electrophysiology work and prosthetics oriented postprocessing algorithm development. In the following paragraphs, we describe some of the potential causes of these variations and their potential implications for prosthetic systems.

What might be the cause for these variations in waveform amplitude? The step changes in waveform amplitude appear, in some cases, to result from abrupt shifts in electrode position caused by head movement. For the nonabrupt variation in waveform shape and RMS noise, we believe there could be a number of factors that may play a significant role, including changes in the cortical environment in response to subject activity, including "brain bounce," changes in intracranial pressure (ICP), and other homeostatic factors. At short-to-intermediate timescales (i.e., longer than bursting periods), Lewicki [15] suggests that array movement, or more specifically changes in the neuron–electrode distance, might play a role in waveform shape change. Fluctuations in the ICP could potentially move the cortex tissue relative to the array (or vice versa). Confirming such a relationship is beyond the scope of this work, though may be of interest in future studies.

Since so few of the high acceleration events were coincident with large changes in waveform amplitude, there is the temptation to dismiss these events as rare and unimportant. However, it is important to note that a practical neural prosthesis will have to operate 24 h a day and 7 days a week. As such, the prosthetic system must be able to recognize the 3–4 abrupt changes that might occur in a week, especially as such systems are used for more ambulatory patients. In fact, in one stretch of $\sim$84 h of recording, we found that there were many tens of events that showed abrupt waveform change coincident with high acceleration movements of the head. Our results are only preliminary, however, and will require more data sets and more animals for comprehensive characterization.

Traditional experimental protocols that utilize discrete, daily recording periods have provided limited information regarding neural recording stability. The daily sampling limits the potential characterization of variations to time scales of either minutes or days. It is important to note that similar variations were not observed, however, in the hour long broadband recordings described in [10]. However, those recordings were made under a more traditional experimental protocol in which a restrained monkey performed a repetitive reaching task. It is possible that the more controlled and consistent environment of those recordings, in contrast to the animal freely behaving in the home cage, produces a more consistent cortical environment (e.g., less "brain bounce," smaller changes in intracranial pressure, etc.) and thus reduced variation in waveform shape.

We have shown examples from preliminary data sets of significant waveform shape and RMS noise variation at all three time scales. Both types of variation can have adverse effects on spike-sorting performance, either through the use of an inappropriate threshold or outright misclassification. The improved statistical characterization of the stability of neural recordings enabled by these new long-duration data sets will allow the principled design and evaluation of sorting algorithms. Tolerance to some instabilities in neural recordings has already been incorporated into sorting algorithms. The short-time-scale variations in spike shape can be addressed by incorporating firing statistics into the spike-sorting algorithm [40] and changes in RMS voltage (from which the threshold is typically derived) can be addressed through adaptive thresholding [25]. Long-term variation, however, may require periodic retraining of the spike-sorting parameters. With such readjustments, experimenters report the ability to track single neurons across months or even years (although experimenters cannot be sure the same neurons are being observed without constant tracking, a capability now available with HermesB). There does not appear to be a consensus on exactly what retraining period is required. Current experiments that use discrete daily recording periods naturally update once per day.

The quality of the trained spike-sorting parameters is paramount. Poor classification parameters, and thus poor classification performance, will affect all aspects of neural prosthetic system performance. This does not imply that systems should retrain arbitrarily often. Frequent retraining can have significant costs. For advanced spike-sorting algorithms [23], the training algorithm is computationally expensive. Although our recent power feasibility study has shown that the power consumption of the algorithm in [23] is small relative to real-time classification, it was assumed that retraining would be required only every 12 h [24]. If a much shorter training period is required, the power consumption of training could quickly become significant, making these advanced algorithms inappropriate for fully integrated and implantable prosthetic systems.

Sorting algorithms with an adaptive training approach that continuously integrates over an extended period, similar to the method proposed in [41], as opposed to discrete retraining, might be the best approach in light of the instability of neural recordings. A suitable adaptive algorithm would have an effective training interval short enough to track variations in waveform shape and background process, without the cost of traditional discrete retraining. The apparent sparsity of abrupt changes in waveform shape due to rapid array movement may reduce the occurrence of a potential problem scenario in which abrupt retraining is required. Nonetheless, the presence of these abrupt changes in waveform shape does suggest that, to maximize spike classification accuracy, any algorithm would benefit from the ability to initiate discrete retraining when step changes in the waveform shape are observed. As these chronic electrode arrays are implanted in amputees (rather than tetraplegics), the head will move substantially. It is worthwhile to note that the space between the brain and the dura is larger in humans than monkeys. Therefore "brain bounce" and other nonstationarities may be a larger issue.

At present, HermesB is in active use supporting a number of experiments, as well as ongoing development to increase recording capabilities. As CF technology and battery energy density improve, recording duration will be expanded. Future generations of HermesB will also incorporate wireless telemetry and more simultaneous recording channels.

APPENDIX

The schematics for the analog signal path and the digital module are shown in Fig. 13(a) and (b). For simplicity, the initial impedance conversion op–amps, reference circuitry, and power conditioning circuits are not shown.

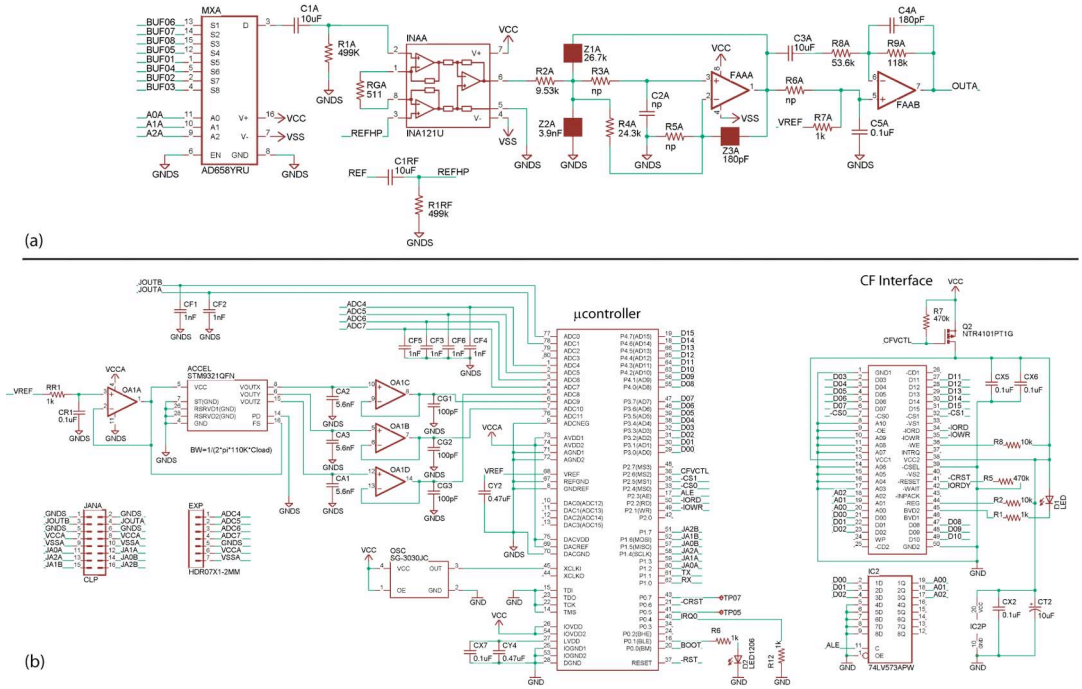

Fig. 13. Schematics for (a) analog signal path (i.e., one of the two channels) and (b) digital module. For simplicity, the initial impedance conversion stage (op–amps in a unity gain configuration) in the analog signal path is not shown. The left most unit is the multiplexer feeding into the high-pass filter, main instrumentation amplifier, secondary amplifiers, and filter. The reference for the instrumentation amplifier is selected via a jumper and is path matched to the neural signal (i.e., passed through an identical high-pass filter). In (b), the left most unit is the three-axis accelerometer, feeding into the microcontroller, along with the neural signals from the analog board. The microcontroller drives the compact flash interface on the far right. Power conditioning circuits are not shown.

ACKNOWLEDGMENT

The authors would like to thank S. Guillory of Intragraphix, who designed and layed out the analog module and layed out the digital module, J. McCrae, K. Merkle, P. Stang, and C. Dunn for their help designing and manufacturing HermesB, M. Risch for expert veterinary care, Dr. A. Mendiola for medical consultation, and S. Eisensee for administrative assistance.

REFERENCES

[1] M. D. Serruya, N. G. Hatsopoulos, L. Paninski, M. R. Fellows, and J. P. Donoghue, "Instant neural control of a movement signal," *Nature*, vol. 416, no. 6877, pp. 141–142, Mar. 2002.

[2] D. M. Taylor, S. I. H. Tillery, and A. B. Schwartz, "Direct cortical control of 3D neuroprosthetic devices," *Science*, vol. 296, pp. 1829–1832, 2002.

[3] J. M. Carmena, M. A. Lebedev, R. E. Crist, J. E. O'Doherty, D. M. Santucci, D. F. Dimitrov, P. G. Patil, C. S. Henriquez, and M. A. L. Nicolelis, "Learning to control a brain-machine interface for reaching and grasping by primates," *PLoS Biol.*, vol. 1, no. 2, pp. 193–208, Oct. 2003.

[4] S. Musallam, B. D. Corneil, B. Greger, H. Scherberger, and R. A. Andersen, "Cognitive control signals for neural prosthetics," *Science*, vol. 305, no. 5681, pp. 258–262, Jul. 2004.

[5] G. Santhanam, S. I. Ryu, B. M. Yu, A. Afshar, and K. V. Shenoy, "A high-performance brain-computer interface," *Nature*, vol. 442, no. 7099, pp. 195–198, Jul. 2006.

[6] L. R. Hochberg, M. D. Serruya, G. M. Friehs, J. A. Mukand, M. Saleh, A. H. Caplan, A. Branner, D. Chen, R. D. Penn, and J. P. Donoghue, "Neuronal ensemble control of prosthetic devices by a human with tetraplegia," *Nature*, vol. 442, no. 7099, pp. 164–171, Jul. 2006.

[7] E. M. Maynard, C. T. Nordhausen, and R. A. Normann, "The Utah intracortical electrode array: A recording structure for potential brain-computer interfaces," *Electroencephalogr. Clin. Neurophysiol.*, vol. 102, no. 3, pp. 228–239, Mar. 1997.

[8] E. M. Maynard, N. G. Hatsopoulos, C. L. Ojakangas, B. D. Acuna, J. N. Sanes, R. A. Normann, and J. P. Donoghue, "Neuronal interactions improve cortical population coding of movement direction," *J. Neurosci.*, vol. 19, no. 18, pp. 8083–8093, Sep. 1999.

[9] N. Hatsopoulos, J. Joshi, and J. G. O'Leary, "Decoding continuous and discrete motor behaviors using motor and premotor cortical ensembles," *J. Neurophysiol.*, vol. 92, pp. 1165–1174, 2004.

[10] S. Suner, M. R. Fellows, C. Vargas-Irwin, G. K. Nakata, and J. P. Donoghue, "Reliability of signals from a chronically implanted, silicon-based electrode array in non-human primate primary motor cortex," *IEEE Trans. Neural Syst. Rehabil. Eng.*, vol. 13, no. 4, pp. 524–541, Dec. 2005.

[11] A. B. Schwartz, "Cortical neural prosthetics," *Ann. Rev. Neurosci.*, vol. 27, pp. 487–507, Jul. 2004.

[12] M. S. Fee, P. P. Mitra, and D. Kleinfeld, "Variability of extracellular spike waveforms of cortical neurons," *J. Neurophysiol.*, vol. 76, no. 6, pp. 3823–3833, Dec. 1996.

[13] J. C. Williams, R. L. Rennaker, and D. R. Kipke, "Stability of chronic multichannel neural recordings: implications for a long term neural interface," *Neurocomputing*, vol. 26–27, pp. 1069–1076, 1999.

[14] X. Liu, D. B. McCreery, L. A. Bullara, and W. F. Agnew, "Evaluation of the stability of intracortical microelectrode arrays," *IEEE Trans. Neural Syst. Rehabil. Eng.*, vol. 14, no. 1, pp. 91–100, Mar. 2006.

[15] M. S. Lewicki, "A review of methods for spike sorting: The detection and classification of neural action potentials," *Network: Comput. Neural Syst.*, vol. 9, no. 4, pp. R53–R78, Nov. 1998.

[16] A. L. Vyssotski, A. N. Serkov, P. M. Itskov, G. Dell'Omo, A. V. Latanov, D. P. Wolfer, and H.-P. Lipp, "Miniature neurologgers for flying pidgeons: Multichannel EEG and action and field potentials in combination with GPS recording," *J. Neurophysiol.*, vol. 95, no. 2, pp. 1263–1273, Feb. 2006.

[17] J. Mavoori, A. Jackson, C. Diorio, and E. Fetz, "An autonomous implantable computer for neural recording and stimulation in unrestrained primates," *J. Neurosci. Methods*, vol. 148, no. 1, pp. 71–77, Oct. 2005.

[18] I. Obeid, M. L. Nicolelis, and P. D. Wolf, "A multichannel telemetry system for single unit neural recordings," *J. Neurosci. Methods*, vol. 133, no. 1–2, pp. 33–38, Feb. 2004.

[19] R. Harrison, P. Watkins, R. Kier, D. Black, R. Normann, and F. Solzbacher, "A low-power integrated circuit for a wireless 100 electrode neural recording system," in *Proc. IEEE Int. Commun. Satellite Syst. Conf.*, 2006, pp. 554–555.

[20] R. E. Isaacs, D. J. Weber, and A. B. Schwartz, "Work toward real-time control of a cortical neural prosthesis," *IEEE Trans. Rehabil Eng.*, vol. 8, no. 2, pp. 196–198, Jun. 2000.
[21] J. Wessberg, C. R. Stambaugh, J. D. Kralik, P. D. Beck, M. Laubach, J. K. Chapin, J. Kim, S. J. Biggs, M. A. Srinivasan, and M. A. L. Nicolelis, "Real-time prediction of hand trajectory by ensembles of cortical neurons in primates," *Nature*, vol. 408, no. 6810, pp. 361–365, Nov. 2000.
[22] K. V. Shenoy, D. Meeker, S. Cao, S. A. Kureshi, B. Pesaran, P. Mitra, C. A. Buneo, A. P. Batista, J. W. Burdick, and R. A. Andersen, "Neural prosthetic control signals from plan activity," *NeuroReport*, vol. 14, no. 4, pp. 591–596, Mar. 2003.
[23] M. Sahani, "Latent variable models for neural data analysis," Ph.D. dissertation, Comput. Neural Syst., California Inst. Technol., Pasadena, CA, May 1999.
[24] Z. S. Zumsteg, C. Kemere, S. O'Driscoll, G. Santhanam, R. E. Ahmed, K. V. Shenoy, and T. H. Meng, "Power feasibility of implantable digital spike sorting circuits for neural prosthetic systems," *IEEE Trans. Neural Syst. Rehabil. Eng.*, vol. 13, no. 3, pp. 272–279, Sep. 2005.
[25] P. T. Watkins, G. Santhanam, K. V. Shenoy, and R. R. Harrison, "Validation of adaptive threshold spike detector for neural recording," in *Proc. 26th Annu. Conf. IEEE Eng. Med. Biol. Soc.*, San Francisco, CA, Sep. 2004, vol. 6, pp. 4079–4082.
[26] J. P. Donoghue, J. N. Sanes, N. G. Hatsopoulos, and G. Gál, "Neural discharge and local field potential oscillations in primate motor cortex during voluntary movements," *J. Neurophysiol.*, vol. 79, no. 1, pp. 159–173, Jan. 1998.
[27] G. Santhanam, M. M. Churchland, M. Sahani, and K. V. Shenoy, "Local field potential activity varies with reach distance, direction, and speed in monkey pre-motor cortex," *Soc. Neurosci. Abstracts*, no. 918.1, Nov. 2003, poster presentation. New Orleans, LA.
[28] A. Destexhe, D. Contreras, and M. Steriade, "Spatiotemporal analysis of local field potentials and unit discharges in cat cerebral cortex during natural wake and sleep states," *J. Neurosci.*, vol. 19, no. 11, pp. 4595–4608, Jun. 1999.
[29] J. Tanji and E. V. Evarts, "Anticipatory activity of motor cortex neurons in relation to direction of an intended movement," *J. Neurophysiol.*, vol. 39, no. 5, pp. 1062–1068, Sep. 1976.
[30] M. Weinrich and S. P. Wise, "The premotor cortex of the monkey," *J. Neurosci.*, vol. 2, no. 9, pp. 1329–1345, Sep. 1982.
[31] M. Weinrich, S. P. Wise, and K. H. Mauritz, "A neurophysiological study of the premotor cortex in the rhesus monkey," *Brain*, vol. 107, no. 2, pp. 385–414, Jun. 1984.
[32] M. Godschalk, R. N. Lemon, H. G. Kuypers, and J. van der Steen, "The involvement of monkey premotor cortex neurons in preparation of visually cued arm movements," *Behav. Brain Res.*, vol. 18, no. 2, pp. 143–157, Nov.–Dec. 1985.
[33] K. Kurata, "Distribution of neurons with set- and movement-related activity before hand and foot movements in the premotor cortex of rhesus monkeys," *Exp. Brain Res.*, vol. 77, no. 2, pp. 245–256, Sep. 1989.
[34] M. M. Churchland, B. M. Yu, S. I. Ryu, G. Santhanam, and K. V. Shenoy, "Neural variability in premotor cortex provides a signature of motor preparation," *J. Neurosci.*, vol. 26, no. 14, pp. 3697–3712, Apr. 2006.
[35] R. R. Harrison, G. Santhanam, and K. V. Shenoy, "Local field potential measurement with low-power analog integrated circuit," in *Proc. 26th Annu. Conf. IEEE Eng. Med. Biol. Soc.*, San Francisco, CA, Sep. 2004, vol. 6, pp. 4067–4070.
[36] R. N. Holdefer and L. E. Miller, "Primary motor cortical neurons encode functional muscle synergies," *Exp. Brain Res.*, vol. 146, no. 2, pp. 233–243, Sep. 2002.
[37] M. M. Morrow and L. E. Miller, "Prediction of muscle activity by populations of sequentially recorded primary motor cortex neurons," *J. Neurophysiol.*, vol. 89, no. 4, pp. 2279–2288, Apr. 2003.
[38] A. Jackson, J. Mavoori, and E. E. Fetz, "Correlations between the same motor cortex cells and arm muscles during a trained task, free behavior and natural sleep in the macaque monkey," *J. Neurophysiol.*, vol. 97, pp. 360–374, 2007.
[39] A. Jackson, C. T. Moritz, J. Mavoori, T. H. Lucas, and E. E. Fetz, "The neurochip BCI: Towards a neural prosthesis for upper limb function," *IEEE Trans. Neural Syst. Rehabil. Eng.*, vol. 14, no. 2, pp. 187–190, Jun. 2006.
[40] C. Pouzat, M. Delescluse, P. Viot, and J. Diebolt, "Improved spike-sorting by modeling firing statistics and burst-dependent spike amplitude attenuation: A Markov chain Monte Carlo approach," *J. Neurophysiol.*, vol. 91, no. 6, pp. 2910–2928, Jan. 2004.
[41] A. Bar-Hillel, A. Spiro, and E. Stark, , L. K. Saul, Y. Weiss, and L. Bottou, Eds., "Spike sorting: Bayesian clustering of non-stationary data," in *Advances in Neural Information Processing Systems 17*. Cambridge, MA: MIT Press, Jan. 2004, pp. 105–112.

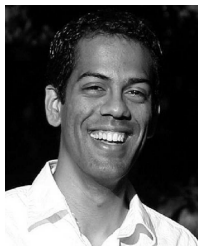

Gopal Santhanam received the B.S. degree in electrical engineering and computer science and the B.A. degree in physics from the University of California, Berkeley, in 1999 and the M.S. and Ph.D. degrees in electrical engineering from Stanford University, Stanford, CA, in 2002 and 2006, respectively.

His research involved neural prosthetics system design, neural signal processing, and embedded neural recording systems. He also has extensive industry experience through various consulting projects involving embedded systems.

Dr. Santhanam is the recipient of notable awards including the National Defense Science and Engineering Graduate fellowship and the National Science Foundation graduate fellowship.

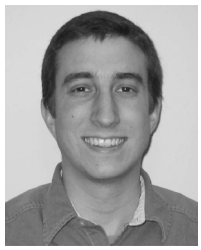

Michael D. Linderman (S'04) received the B.S. degree in engineering from Harvey Mudd College, Claremont, CA, in 2003 and the M.S. degree in electrical engineering from Stanford University, Stanford, CA, where he is currently working toward the Ph.D. degree in electrical engineering.

His research interests are multiprocessor architectures and programming models for neural prosthetic systems and other challenging information processing problems.

Mr. Linderman is the recipient of the of the National Defense Science and Engineering Graduate Fellowship and Stanford Graduate Fellowship.

Vikash Gilja received the S.B. degrees in electrical engineering and computer science and brain and cognitive sciences and the M.Eng. degree in electrical engineering and computer science from the Massachusetts Institute of Technology, Cambridge, MA, in 2003 and 2004, respectively. Currently, he is working towards the Ph.D. degree in computer science at Stanford University, Stanford, CA.

At Stanford, he joined the Neural Prosthetics Laboratory. His research interests center around the design of practical and robust neural prosthetics systems.

Mr. Gilja is the recipient of awards and honors including the National Defense Science and Engineering Graduate Fellowship and the National Science Foundation Graduate Fellowship.

Afsheen Afshar (S'99) received the B.S.E. degree in electrical engineering and a Certificate in engineering biology from Princeton University, Princeton, NJ, in 2002 and the M.S. in electrical engineering from Stanford University, Stanford, CA, in 2005, where he is currently working towards the M.D. and Ph.D. degrees in electrical engineering.

His research involves improving neural prosthesis performance, developing better neural processing algorithms, and helping further the understanding of the Parkinsonian brain.

Mr. Afshar received the Medical Scientist Training Program (MSTP) Fellowship and the Bio-X Fellowship.

Stephen I. Ryu received the B.S. and M.S. degree in electrical engineering from Stanford University, Stanford, CA, in 1994 and 1995, respectively, and the M.D. degree from the University of California at San Diego, La Jolla, in 1999. He completed neurosurgical residency and fellowship training at Stanford University in 2006.

Currently, he is an Assistant Professor at the Department of Neurosurgery, Stanford University. His research interests include brain-machine interfaces, neural prosthetics, spine biomechanics, and stereotactic radiosurgery.

Teresa H. Meng (S'82–M'83–SM'93–F'99) received the Ph.D. degree in electrical engineering and computer science from the University of California, Berkeley, in 1988.

She is the Reid Weaver Dennis Professor of Electrical Engineering at Stanford University, Stanford, CA. Her research activities during the first ten years at Stanford included low-power circuit and system design, video signal processing, and wireless communications. In 1999, she took leave from Stanford University and founded Atheros Communications, which delivers the core technology for high-performance wireless communication systems. She returned to Stanford University in 2000 to continue her research and teach. Her current research interests focus on neural signal processing and computation architectures for future scaled CMOS technology. She is the author of one book, several book chapters, and over 200 technical articles in journals and conferences.

Dr. Meng has received many awards and honors for her research work at Stanford including an National Science Foundation Presidential Young Investigator Award, an Office of Naval Research Young Investigator Award, an IBM Faculty Development Award, a Best Paper Award from the IEEE Signal Processing Society, the Eli Jury Award from the University of California, Berkeley, and awards from AT&T, Okawa Foundation, and other industry and academic organizations. As a result of founding Atheros Communications, she was named one of the Top 10 Entrepreneurs in 2001 by Red Herring, Innovator of the Year in 2002 by MIT Sloan School eBA, and the CIO 20/20 Vision Award in 2002.

Krishna V. Shenoy (S'87–M'01–SM'06) received the B.S. degree in electrical engineering from the University of California, Irvine, in 1990, and the S.M. and Ph.D. degrees in electrical engineering and computer science from the Massachusetts Institute of Technology, Cambridge, in 1992 and 1995, respectively.

He was a Systems Neuroscience Postdoctoral Fellow in the Division of Biology, California Institute of Technology, Pasadena, from 1995 to 2001. He joined the Faculty of Stanford University, Stanford, CA, in 2001, where he is currently an Assistant Professor at the Department of Electrical Engineering and Neurosciences Program. His current research activities include neurophysiological investigations of sensorimotor integration and coordination, neural prosthetic system design, and neural signal processing and electronics.

Dr. Shenoy is the recipient of awards and honors including the 1996 Hertz Foundation Doctoral Thesis Prize, a Burroughs Wellcome Fund Career Award in the Biomedical Sciences, the William George Hoover Faculty Scholar in Electrical Engineering at Stanford University, the Robert N. Noyce Family Scholar in the Stanford University School of Engineering, an Alfred P. Sloan Research Fellow and a Defense Science Research Council Fellow. He is also an American Physical Society (APS) member.